ISSN 2070-2051, Protection of Metals and Physical Chemistry of Surfaces, 2016, Vol. 52, No. 1, pp. 66–73. © Pleiades Publishing, Ltd., 2016.
Original Russian Text © L.N. Shirokova, V.A. Alexandrova, A.A. Revina, 2016, published in Fizikokhimiya Poverkhnosti i Zashchita Materialov, 2016, Vol. 52, No. 1, pp. 64–71.

NANOSCALE AND NANOSTRUCTURED MATERIALS AND COATINGS

The Structure and Composition of Iron Nanoparticles Stabilized by Carboxymethyl Chitin Resulting from Ultrasonic Irradiation

L. N. Shirokova[a], V. A. Alexandrova[a], and A. A. Revina[b]

[a] *Topchiev Institute of Petrochemical Synthesis, Russian Academy of Sciences, Moscow, 119991 Russia*

[b] *Frumkin Institute of Physical Chemistry and Electrochemistry, Russian Academy of Science, Moscow, 119071 Russia*

e-mail: shirokova@ips.ac.ru, alexandrova@ips.ac.ru

Received February 13, 2015

Abstract—The methods of sonochemistry and "green" nanotechnology were used to develop a single-stage process to transfer iron nanoparticles from their micellar solution in isooctane to aqueous solution of carboxymethyl chitin excluding an intermediate stage of producing iron nanoparticulate dispersion in water. The structure and dimensions of iron nanoparticles in a macromolecular system based on 6-O-carboxymethyl chitin were examined using X-ray microanalysis and selected-area electron diffraction analysis, transmission electron microscopy (TEM), and atomic force microscopy (AFM). According to TEM and AFM data, the sizes of ultradispersed particles were within the range of 2–4 nm. The X-ray investigations indicated that iron nanonoparticles in the carboxymethyl chitin–iron nanoparticles system consisted mainly of zero-valent alpha-iron particles (α-Fe^0) and a number of magnetite Fe_3O_4 nanoparticles. Because both types of particles exhibit magnetic properties, these metal–polymer nanocomposites may have a wide range of applications in medicine, electronics, biotechnology, ecology, and catalysis.

DOI: 10.1134/S2070205116010202

INTRODUCTION

The biocompatibility, biodegradability, nontoxicity, film- and fiber-forming ability, and low cost of chitin and chitosan are attracting the attention of researchers to these polysaccharides in various fields of science and technology, including medicine, bioinspired material science, and pharmacy [1, 2]. Chitin is insoluble in conventional solvents, and this fact constrains its practical applications, while the N-deacetylated chitin derivative chitosan dissolves in aqueous solutions only in acid conditions. One method used to increase the solubilities of chitin and chitosan is their chemical modification. The best way to increase the water solubility of chitin over a wide range of pH is to introduce carboxymethyl group CH_2COOH, resulting in a useful biological activity.

The functional group gives 6-O-carboxymethyl chitin the ability to serve as a carrier matrix for delivery of DNA, proteins, medical products, and high-activity nanosized particles [3].

Zero valent iron nanoparticles can be prepared in aqueous solutions by reduction of ions Fe^{2+} or Fe^{3+} by sodium tetrahydroborate $NaBH_4$ or by thermal destruction of iron pentacarbonyl $Fe(CO)_5$ in organic solvents or argon [5]. The aggregative instability is a specific feature of nanosized particles in solutions. The loss of aggregative instability to a dispersed system leads to spontaneous particle coarsening due to coagulation, and, as a consequence, the functional properties of nanoparticles and materials based on nanoparticles deteriorate. Therefore, the practical use of solutions of nanoparticles may involve their stabilization realized through the surface coating of a particle "core," introduction of a stabilizer into solution, selection of solvent, and etc. A prevalent method is reduction of ferric salts with sodium tetrahydroborate $NaBH_4$ and stabilization of zero-valent nanosized iron particles within the inverted micelles of surfactant [6] and in a matrix based on polyacrylic acid, PEG, PVA, starch, agar–agar, sodium alginate, and dextrane, as well as cellulose, chitosan, and their derivatives [7–13].

The reaction scheme for boron hydrogenation method of reduction of iron ions in water appears as follows:

$$Fe^{2+} + 2BH_4^- + 6H_2O \rightarrow Fe^0 + 2B(OH)_3 + 7H_2. \quad (1)$$

The most important advantages of inverted micelles used for synthesis of metal nanoparticles are the ability to prepare the homogeneous particles with a narrow size distribution within several nanometers and the ability to control the growth of nanoparticles by changing the extent of hydration (solubilization) $\omega = [H_2O]/[\text{hydrocarbon}]$ [14].

Application of iron nanoparticles to prepare hydrophobic nanocomposite materials in the forms of films, fibers, etc., required to combine nanoparticles with solution of hydrophobic polymer arises. In this regard, it is interesting to carry out a work on preliminary production of zero-valent iron particles by $NaBH_4$ reduction of ferric salts in alcohol solution of bromide cetyl-

trimethyl-ammonium and their further dispergation in acetone solution of acetylcellulose [15]. It should be noted that, although chemical reduction is a simple and convenient preparative method, the compounds that are commonly used as reducing agents (boron hydride, hydrazine, formamide) are toxic to the environment [16]. Moreover, metal nanoparticles prepared by chemical reduction often contain impurities of starting reagents and coproducts. For this reason, the iron nanoparticles used in this work were synthesized by the radiation-chemical method in the inverted micelles of a synthetic structural analog of native lipids sodium 1,4-bis-[(2-ethylhexyl)oxy]-1,4-dioxobutane-2-sulfonate (Aerosol-OT or AOT) $C_{20}H_{37}O_7SNa$ [17].

When iron nanoparticles are used to prepare hydrophilic nanocomposite materials, it is necessary to combine nanoparticles with polymer solution in water. This requires a preliminary extraction of metal nanoparticulate dispersion in water from their micellar solution in hydrocarbon. However, this process entails a long-term keeping of heterophase system until a sharp separation between the organic and water layers is achieved. In addition, this process is related to a loss of particles due their oxidation and destabilization.

With this in mind, the aim of the present work is to develop a single-stage process to transfer iron nanoparticles from their micellar solution in isooctane to aqueous solution of carboxymethyl chitin excluding the intermediate stage of preparation of iron nanoparticulate dispersion in water. To achieve this goal, ultrasonic treatment of a heterophase isooctane–water system containing iron nanoparticles and polymer was employed. The task of the work included also detailed examination of the morphology of iron nanoparticles in the carboxymethyl chitin matrix using X-ray microanalysis, selected-area electron diffraction analysis, TEM, and AFM.

EXPERIMETAL

Materials

Chitin (1 → 4)-2-acetamido-2-deoxy-β-D-glucan prepared from crab shell with $M = (40–45) \times 10^4$ (Bioprogress, Russia) was used in the work.

Sodium hydroxide (chemically pure), 2-isopropanol (ASC reagent), and chloroacetic acid (chemically pure) were utilized without preliminary cleaning. Micellar solution of iron nanoparticles in isooctane (Lanakom, Russia) was used as a source of nanoparticles [17]. Nanosized iron species were prepared by the radiation-chemical reduction of iron ions Fe^{2+} with active reducing radiolysis particles (solvated electrons, monoatomic hydrogen or other radicals) generated by γ-^{60}Co in the inverted micellar system $FeSO_4 \cdot 7H_2O$–H_2O–AOT–isooctane). To prepare water-organic micellar solution of iron nanoparticles, 0.15 M AOT (Acros Organics), 0.3 M $FeSO_4 \cdot 7H_2O$ (analytically pure) and isooctane (analytically pure) were used. To remove oxygen, the prepared solutions were preliminarily blown off with argon or helium. The irradiation dose was 10 kGy, and the degree of hydration was $\omega = [H_2O]/[AOT] = 4.0$.

METHODS

Synthesis of carboxymethyl chitin

Water soluble 6-O-carboxymethyl chitin (CMC) with molecular mass of 8×10^4 and a degree of carboxylation of 1.0 was prepared from chitin according to the method of [18].

Synthesis of iron nanoparticles embedded into carboxymethyl chitin matrix using ultrasonic irradiation

For ultrasonic irradiation, water solution of CMC (0.5–2.0 wt %) was kept in a vessel; a required amount of micellar solution of iron nanoparticles in isooctane by different ratios with consideration of optical density of nanoparticles was added portionwise without mixing. The ultrasonic irradiation of the heterophase systems was carried out using a UZO-ST setup (Reltek, Russia) operating at 44 kHz. The insonation time was varied from 5 to 20 min. The solutions under study were ice cooled in order to avoid an elevation of temperature higher than 20°C under ultrasonic irradiation.

Method of analysis

Quantitative determination of content of iron particles in going from the organic phase to the aqueous one and determination of their stability in the CMC matrix were conducted by measuring the absorption intensity of iron nanoparticles at 290 nm using a UV-Vis SPECORD M-40 spectrophotometer (Carl Zeiss, Germany) in a quartz cell with an optical path length of 1 mm at 20°C. For measurements, 0.15 M AOT/isooctane solution and bidistilled water were used as reference solutions.

Morphological analysis of iron nanoparticles in CMC matrix

The presence of metal nanoparticles and their sizes were evaluated by TEM using a Tecnai electron microscope (Phillips Electron Optics, Holland). The X-ray microanalysis unit was included into the Tecnai electron microscope.

The samples for TEM measurements were prepared by freezing with following removal of water by vacuum evaporation in solid state. A drop of iron nanoparticles in CMC was placed at a microscope slide cooled up to liquid-nitrogen temperature. The sample was immediately frozen. Afterward, the micro-

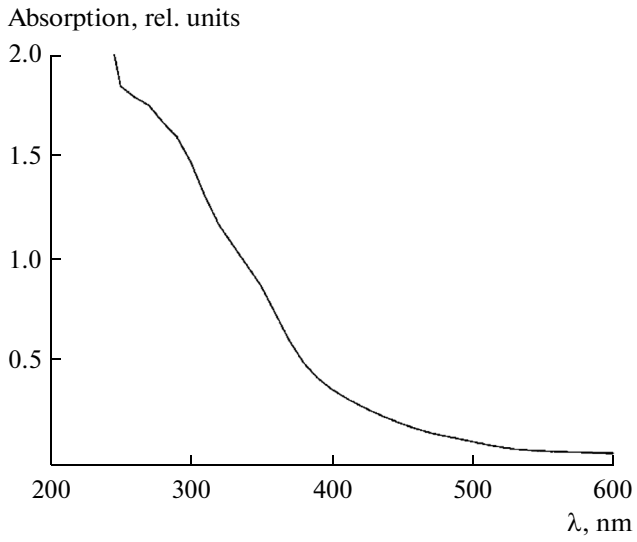

Fig. 1. Electron spectra of micellar solution of iron nanoparticles in isooctane. Hydration extent ω = 4.0.

scope slide was placed into a high vacuum exhaust post where water evaporated from the frozen sample. A copper grid was put on the surface of the sample in the usual manner. After separation of the copper grid with the species under study from the microscope slide, the sample was examined by the TEM method with the use of selected-area electron diffraction and microprobe electron analysis.

A BerMad 2000 atomic force microscope (Nanotec Electronica, Spain) was used to determine the sizes of nanoparticles. An NSG10 silicon cantilever (NT-MDT, Russia) with a length of 100 μm, cross section of 35 × 2 μm operating at a resonance frequency of 255 kHz, and tip curvature radius of 10 nm or less) was employed.

An important issue for atomic force microscopy is related to the support for a sample and the conditions of sample deposition on it. When employing a glass substrate with indium tin oxide (ITO) coating, aggregates of iron nanoparticles are formed at the ITO surface [19]. Therefore, it was decided to use an atomically smooth mica substrate in this work. The mica surface had such a roughness such that it enabled one to obtain a depth resolution of no less than 0.4 nm.

Surfactant (AOT) molecules on the surface of iron nanoparticles obtained in inverted micelles are a significant impediment to determination of the actual size of nanoparticles. Therefore, a special sedimentation technique was used for nanoparticles from micellar solution on the mica surface (spin coating). This method involves depositing a layer of solution onto the center of a mica surface fixed on a rotating substrate and then spinning the substrate; excess solution substrate is removed. and the sample is dried at 30°C [19]. Afterward, the obtained film was treated with distilled water in order to visualize single metal nanoparticles on the mica surface.

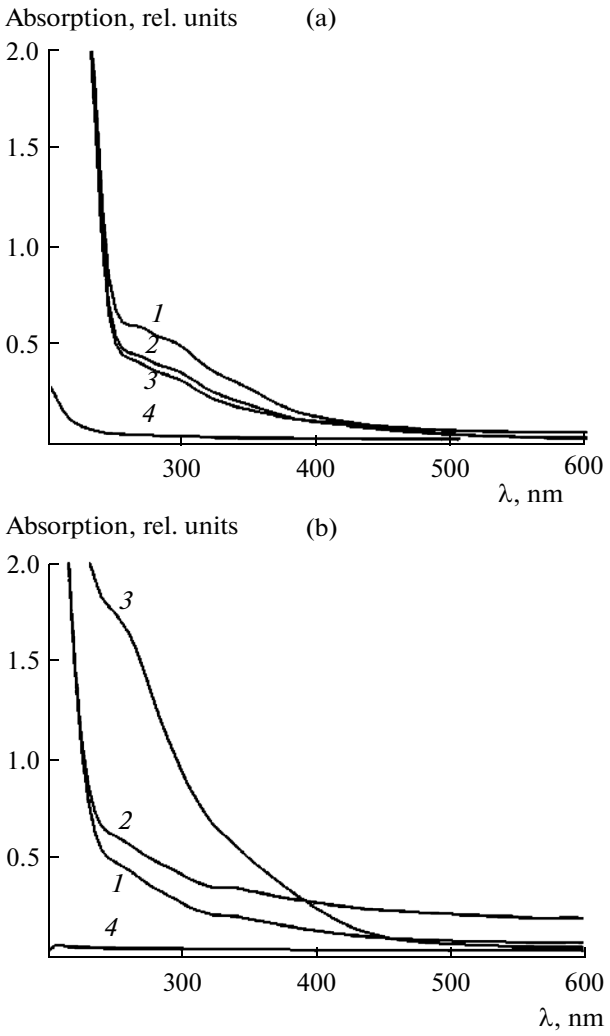

Fig. 2. Electron spectra of iron nanoparticles in the CMC–iron nanoparticles heterophase system after ultrasonic irradiation for 5 (curves *1*a and *1*b), 10 (curves *2*a and *2*b), and 20 min (curves *3*a and *3*b) in (a) an organic micellar layer and (b) in water solution of CMC, respectively, at exposure for 1 day; curves *4*a and *4*b show the electron spectra for AOT/isooctane and bidistilled water, respectively.

RESULTS AND DISCUSSION

Figure 1 shows the electron spectra of a micellar solution of iron nanoparticles in isooctane. The absorption band at 290 nm is typical for iron nanoparticles and is associated with a surface (localized) plasmon resonance of metal nanoparticles. Colloid particles with hydration extent ω = 4 were chosen for further investigations, since, at this value of ω, the absorption bands attributed to nanoparticles were most intense and stable in time.

Synthesis of Iron Nanoparticles in CMC Matrix and Investigations of Them by UV-VIS Spectroscopy

Ultrasonic (US) irradiation is used for emulsifying poorly mixed fluids [20–22]. Moreover, ultrasonic

irradiation accelerates and activates heterogeneous reactions. In order to obtain a macromolecular nanosystem including CMC and iron nanoparticles, US processing of the heterophase system was used to move iron nanoparticles from their micellar solution in isooctane to an aqueous solution of CMC. Iron nanoparticles can be modified via adsorption on a solid support as silica gels or carbon nanotubes [17, 23]. However, these particles are insoluble in water and in other polar solvents without additional modification of their surface. In previous investigations, water suspension of metal nanoparticles based on micellar solution of nanoparticles in isooctane was used to introduce metal nanoparticles into water solution of polymer [24]. Whereas the process of aqueous dispersion of metal nanoparticles is associated with a certain loss of nanoparticles due to their oxidation and destabilization, the CMC–iron nanoparticles systems were prepared by means of moving iron nanoparticles from their micellar solution directly to an aqueous solution of polymer (0.5–2.0 wt %) using ultrasonic irradiation of the heterophase system.

The data in Figs. 1, 2a, and 2b give evidence that ultrasonic irradiation of the isooctane–water heterophase system caused a fundamental decrease in the optical density of iron nanoparticles in an upper layer composed of a micellar solution of iron nanoparticles in isooctane. The increase in the ultrasonic irradiation time promoted a decrease in content of nanoparticles in the upper layer and a growth of their amount in the low layer, the aqueous solution of CMC. The decrease of amounts of iron nanoparticles in the upper organic layer and the increase of their content in the low aqueous layer were found from the ratio of the optical density in initial micellar solution in isooctane and after ultrasonic irradiation (table). It follows from the data given in the table that the decrease in the amount of iron nanoparticles in isooctane resulted from ultrasonic irradiation of the heterophase system caused a symbate increase of the absorption bands' intensities attributed to iron nanoparticles in aqueous solution of polymer. The extended duration of ultrasonic treatment brought about more complete transfer of iron nanoparticles to aqueous solution of CMC.

FTIR spectroscopy was used to establish that, due to a system of hydrogen bonds existing between the –N–H bond in the amide group of CMC and –C=O in the ester group of the surfactant stabilizer of iron nanoparticles, three-component systems composed of a core formed by iron nanoparticles that are stabilized by hydrophobic surfactant and hydrophilic CMC [25] were formed. It should be noted that the value of optical density of iron nanoparticles in composite films remained constant over 6 months.

The scheme of CMC synthesis, transport of iron nanoparticles from micellar solution of iron nanoparticles in isooctane to aqueous solution of CMC under action of ultrasonic irradiation, and their bonding due to formation of a system of hydrogen bonds is given below:

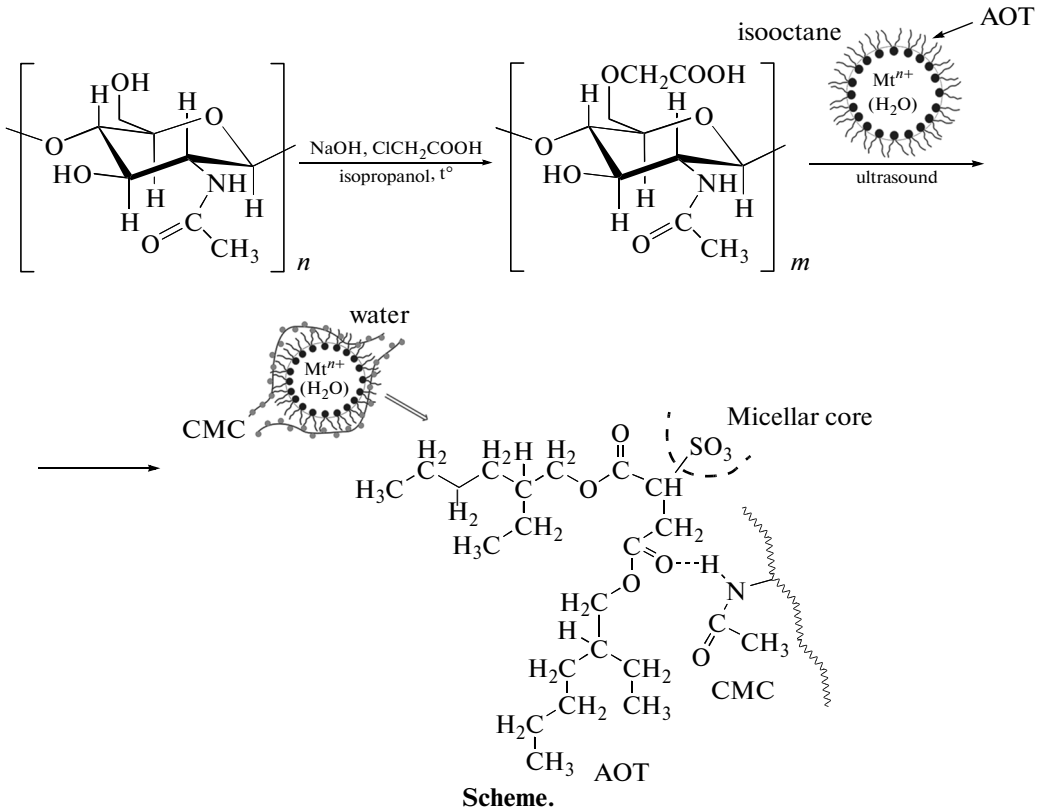

Scheme.

Influence of ultrasonic processing conditions for the CMC–iron nanoparticles heterophase system and the exposure time for this system on the content of iron nanoparticles in micellar solution and in 0.5 wt % CMC solution in the absorption region at 290 nm, pH 7.5.

Exposure time after ultrasonic irradiation, days	Content of iron nanoparticles, %					
	Duration of ultrasonic irradiation, min					
	5	10	20	5	10	20
	organic layer			water layer		
1	72.46	50.72	43.48	22.18	38.10	52.08
7	38.99	23.19	21.74	52.08	65.63	77.30
14	10.0	16.42	8.04	88.96	81.67	90.63

Polymer acts in this system not only as a film-forming material, but also performs the function of a stabilizer of iron particles and modifying agent that changes the affinity of the surface of hydrophobic iron nanoparticles to water molecules [25].

Size and Morphology of Iron Nanoparticles

Figure 3 shows electron microphotographs of iron nanoparticles (0.06 wt % per CMC) in the composition with 0.5 wt % CMC. Iron nanoparticles obtained in CMC solution are spherical. The particle size distribution was evaluated using more than 450 species shown in TEM images (Fig. 3b). The average diameter of particles was 2.2 nm, and the standard deviation was 0.87 nm. The curve of particle size distribution (Gaussian curve) based on the data corresponded to that for a normal distribution and had a monomodal character. The microdiffraction pattern shows the data corresponding to a crystal pattern of alpha-iron in the zero-valent state α-Fe^0 (Fig. 3c).

In addition to the TEM technique, a scanning probe microscope in the AFM mode was used to examine the morphology of particles. Figure 4 shows 2D AFM images, the topographic profile, and 3D AFM images of a film surface prepared from aqueous solution of CMC (a, d, g), micellar solution of iron nanoparticles with hydration extent $\omega = 4$ (b, e, h) and the CMC–iron nanoparticles system (c, f, i), respectively. Scanning was done in a semi-contact mode.

The lateral dimensions of iron nanoparticles less than 10 nm could be barely determined using a cantilever of 10-nm radius, and, probably, due to incomplete removal of AOT stabilizer molecules. Therefore, in further discussion of the dimensions of nanoparticles, only their dimensions along the Z axis were con-

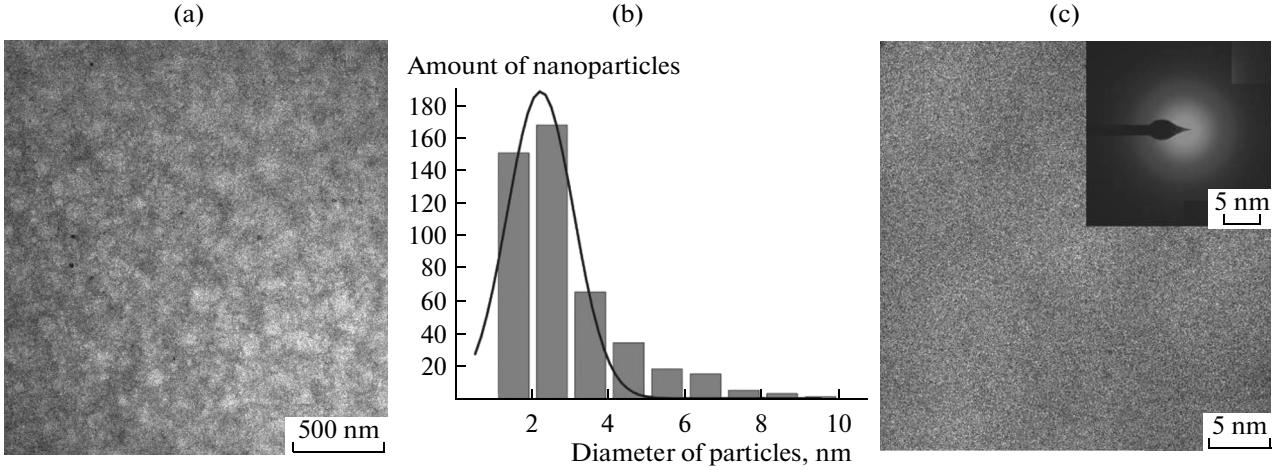

Fig. 3. (a) Electron microphotography of iron nanoparticles (0.06 wt % with respect to CMC) in composition with 0.5 wt % CMC and (b) the size distribution histogram of iron nanoparticles; (c) electron microphotographs of iron nanoparticles (0.06 wt % with respect to CMC) in composition with 0.5 wt % CMC (hundredfold magnification) and corresponding microdiffraction pattern.

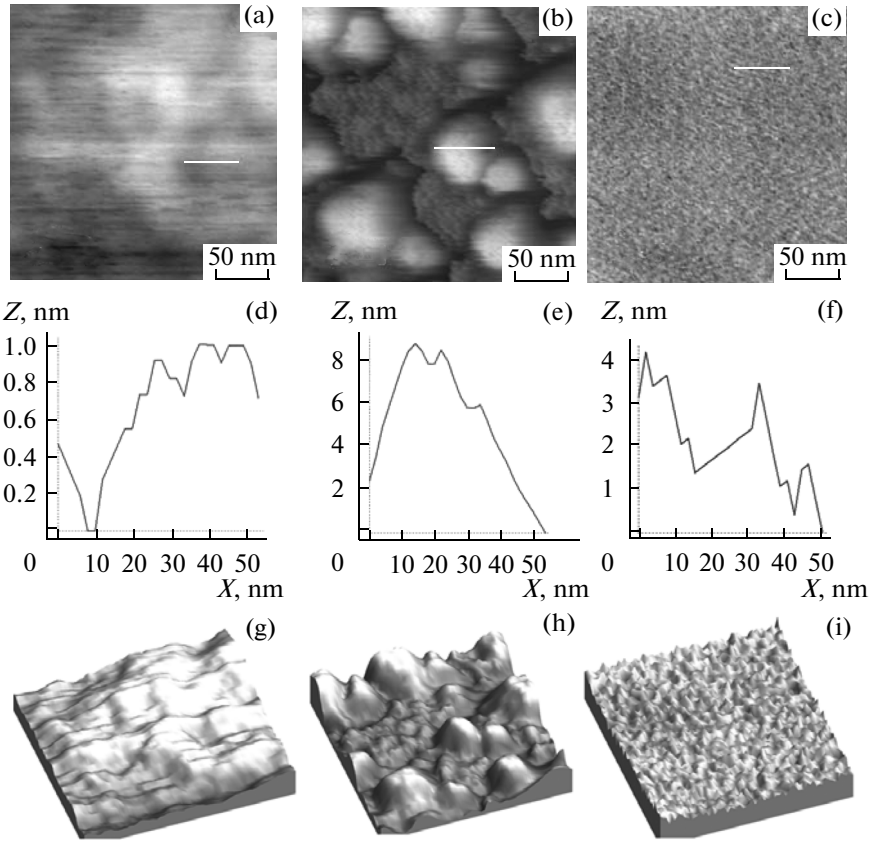

Fig. 4. 2D AFM images, topographic profile, and 3D AFM images of film surfaces formed from (a, d, g) CMC aqueous solution; (b, e, h) micellar solution of iron nanoparticles with hydration extent $\omega = 4$; and(c, f, i)CMC–iron nanoparticles system, respectively.

sidered. AFM-image of the film prepared from 0.5 wt % CMC system (Fig. 4a, 4d, 4g) by spin-coating indicated the formation of a CMC layer with the roughness of about 1 nm, which depended on the applied voltage, the time of sedimentation, and the concentration of polysaccharide.

As follows from the data in Figs. 4c and 4f, iron nanoparticles in the CMC–iron nanoparticles system are homogeneously distributed within the CMC film and the size of particles are within the range of 3–4 nm, while the size of iron nanoparticles in micellar solution attained 9 nm (Figs. 4b, 4e, 4h). The increase in size of iron nanoparticles is likely associated with trace amounts of surfactant molecules (AOT), which prevent the determination of actual size of nanoparticles.

It should be noted that the size of iron nanoparticles in the CMC–iron nanoparticles system determined by the TEM technique coincides with the value found from AFM data.

Coupled with this, the film surface prepared from the CMC–iron nanoparticles system is rougher than that prepared separately from CMC and from iron nanoparticles.

This may be due to chelating and film-forming characteristics of hydrophilic CMC, which is able to envelop nanoparticles and adsorb on the surface of iron nanoparticles, preventing their aggregation. Thus, the process of transfer of iron nanoparticles from their micellar solution in isooctane to aqueous solution of CMC by means of the ultrasonic treatment of heterophase system exerted a significant effect on the morphology of iron nanoparticles.

It was established that the size of iron nanoparticles in both micellar solution and the CMC–iron nanoparticles systems could vary over time increasing, within the range of 3–20 nm.

Thus, Figs. 5a and 5c shows aggregated iron nanoparticles surrounded with a 0.5 wt % CMC layer and their diffraction patterns.

It can be concluded based on the results of X-ray microanalysis (Fig. 5) that the composition of iron nanoparticles in the CMC–iron nanoparticles composite involved mainly alpha-iron particles in the zero-valent state α-Fe^0 (Fig. 5a) with a body-centered cubic lattice. According to results obtained previously [4, 15, 26, 27], α-Fe^0 nanoparticles can be used for reduction degradation of environmental contaminants as chlorine and nitrogen-containing organic solvents and pesticide chemicals, colorants, and heavy-metal ions. Moreover, some amount of the crystalline

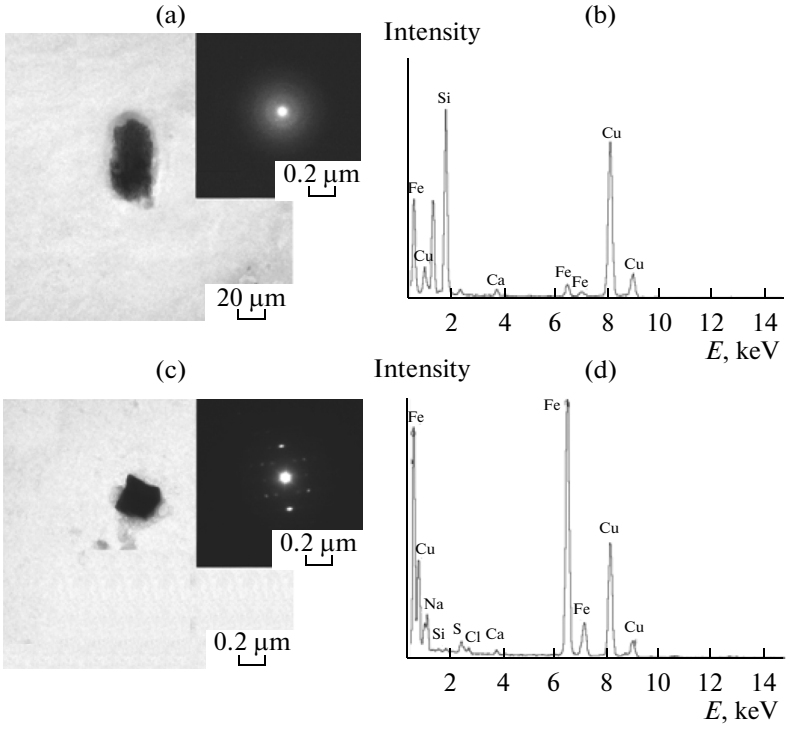

Fig. 5. Electron microphotographs and corresponding microdiffraction pattern and micro X-ray pattern of films obtained from aqueous solutions of the CMC–iron nanoparticles system: (a, b) α-Fe^0 and (c, d) and Fe_3O_4.

phase of iron oxide (magnetite) was found in the CMC–iron nanoparticles system (Fig. 5b). Nanoparticles Fe_3O_4 exhibited pronounced magnetic properties and are characterized by a face-centered cubic lattice and an inverse spinel structure $(Fe_8^{3+})_t[Fe_8^{3+}Fe_8^{2+}]_oO_{32}$ [28] formed by 32 O^{2-} ions placed along the 111 direction, where a third of cations Fe^{3+} occupies tetrahedral sites (t), while equal numbers of ions Fe^{3+} and Fe^{2+} occupy octahedral sites (o).

The microdiffraction pattern in Fig. 5 indicated trace amounts of Ca, Na, Mg, and Cu present in iron nanoparticles. The presence of Cu species in microdiffraction patterns was caused by the copper grid used as the substrate in preparation of the samples. Occurrence of Ca species in composition of iron particles (Fig. 5) can be caused by the presence of this metal in the structure of the chitin used in CMC synthesis. Salts of Ca^{2+}, Mg^{2+}, Na^+, and other metals originating from seawater were found in the polymorphic form of chitin extracted from different prawn species, as has been shown in a number of recent investigations [29, 30]. Inorganic salts associated with chitin make the crustaceous skeleton hard. Moreover, ion Ca^{2+} and some other metals can serve as cross-linking agents in generation of a complex between α-chitin and protein. Generation of these complexes in the form of a dense layer is required to protect crustaceans from mechanical attack and changes in the temperature and pressure of the environment.

CONCLUSIONS

Single-stage transfer of iron nanoparticles from their micellar solution in isooctane to aqueous solution of carboxymethyl chitin was developed excluding the intermediate stage of preparation of water dispersion of iron nanoparticles.

Macromolecular systems based on CMC and iron nanoparticles with particle size 2–4 nm contain α-iron in the zero-valent state α-Fe^0 and magnetite Fe_3O_4. Nanoparticles of α-Fe^0 can be used in production of functional nanomaterials to protect the environment as reductants of contaminants up to nontoxic compounds.

In addition, Fe_3O_4 nanoparticles with more pronounced magnetic properties may be applicable in biomedicine (biosensors, magnetic resonance imaging, biomolecular markers, controlled local hyperthermia in tumor treatment, bioseparation, etc.).

ACKNOWLEDGEMENTS

We are grateful to V.T. Dubinchuk (Fedorovsky All-Russian Scientific Research Institute of Mineral Resources) for TEM experiments and selected-area electron diffraction analysis.

REFERENCES

1. Jayakumar, R., Menon, D., Manzoor, K., et al., *Carbohydr. Polym.*, 2010, vol. 82, p. 227.

2. Shukla, S.K., Mishra, A.K., Arotiba, O.A., and Mamba, B.B., *Int. J. Biol. Macromol.*, 2013, vol. 59, p. 46.
3. Jayakumar, R., Prabaharan, M., Nair, S., et al., *Prog. Mater Sci.,* 2010, vol. 55, p. 675.
4. Zhang, W., *J. Nanopart. Res.*, 2003, vol. 5, nos. 3–4, p. 323.
5. Karlsson, M.N.A., Deppert, K., Wacaser, B.A., et al., *Appl. Phys. A: Mater. Sci. Process*, 2005, vol. 80, p. 1579.
6. Ibrahem, Moghny, T.A., Mustafa, Y.M., et al., *ISRN Soil Sci.,* 2012, vol. 2012, art. ID 270830.
7. Cirtiu, C.M., Raychoudhury, T., Ghoshal, S., and Moores, A., *Colloids Surf., A*, 2011, vol. 390, p. 95.
8. Lv, X., Jiang, G., Xue, X., et al., *J. Hazard. Mater.*, 2013, vol. 262, p. 748.
9. Wang, X., Le, L., Alvarez, P.J.J., et al., *J. Taiwan Inst. Chem. Eng.*, 2015, vol. 50, p. 297.
10. Kim, H., Hong, H.-J., Jung, J., et al., *J. Hazard. Mater.*, 2010, vol. 176, p. 1038.
11. Ding, Q., Qian, T., Liu, H., and Wang, X., *Appl. Mech. Mater.,* 2011, vols. 55–57, p. 1748.
12. Suguna, M., Kumar, N., Sreenivasulu, V., and Krishnaiah, A., *Sep. Sci. Technol.*, 2014, vol. 49, p. 1613.
13. Kustov, L.M., Finashina, E.D., Shuvalova, E.V., et al., *Environ. Int.*, 2011, vol. 37, p. 1044.
14. Petit, C., Lixon, P., and Pileni, M.-P., *J. Phys. Chem.*, 1993, vol. 97, p. 12974.
15. Wu, L., Shamsuzzoha, M., and Ritchie, S.M.C., *J. Nanopart. Res.*, 2005, vol. 7, nos. 4–5, p. 469.
16. Maneerung, T., Tokura, S., and Rujiravanit, R., *Carbohydr. Polym.*, 2008, vol. 72, p. 43.
17. Revina, A.A., RF Patent 2312741, 2007.
18. Wongpanti, P., Sanchavanakit, N., Supaphol, P., et al., *Macromol. Biosci.*, 2005, vol. 5, p. 1001.
19. Revina, A.A., Daineko, S.V., Bol'shakova, A.N., et al., *Naukoemkie Tekhnol.*, 2011, vol. 12, no. 6, p. 68.
20. Martin-Aranda, R.M. and Calvino-Casilda, V., *Recent Pat. Chem. Eng.*, 2010, vol. 3, p. 82.
21. Miethchen, R., *Ultrasonics*, 1992, vol. 30, p. 173.
22. Suslick, K.S., Doktycz, S.J., and Flint, E.B., *Ultrasonics*, 1990, vol. 28, p. 280.
23. Shvetsov, A.A., Lebedeva, M.V., and Revina, A.A., *Usp. Khim. Khim. Tekhnol.*, 2012, vol. 26, no. 7, p. 18.
24. Shirokova, L.N., Alexandrova, V.A., Egorova, E.M., and Vihoreva, G.A., *Appl. Biochem. Microbiol.*, 2009, vol. 45, p. 422.
25. Alexandrova, V.A., Shirokova, L.N., and Revina, A.A., *Polym. Sci., Ser. B*, 2010, vol. 52, no. 9–10, p. 621.
26. Naja, G., Halasz, A., Thiboutot, S., et al., *Environ. Sci. Technol.*, 2008, vol. 42, p. 4364.
27. Balamurugan, D., Udayasooriyan, C., Vinoth Kumar, K., et al., *Environ. Ecol. Res.*, 2014, vol. 2, p. 291.
28. Laurent, S., Forge, D., Port, M., et al., *Chem. Rev.*, 2008, vol. 108, p. 2064.
29. Cárdenas, G., Cabrera, G., Taboada, E., and Miranda, S., *J. Appl. Polym. Sci.*, 2004, vol. 93, p. 1876.
30. Muzzarelli, R.A.A., *Chitin*, Oxford, UK: Pergamon, 1977.

Translated by E. Khozina